

Identification of the structural damage mechanism of BFRP bars reinforced concrete beams using smart transducers based on time reversal method

Lingzhu Zhou^{a,b}, Yu Zheng^{a,*}, Gangbing Song^c, Dongdong Chen^b, Yuxiao Ye^d

^a School of Environment and Civil Engineering, Dongguan University of Technology, Dongguan 523080 China

^b Key Laboratory of Coastal and Offshore Engineering, Dalian University of Technology, Dalian 116024, China

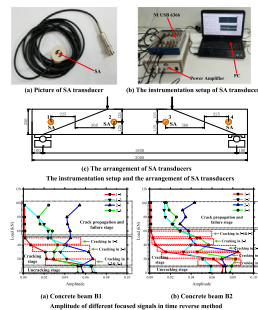
^c Department of Mechanical Engineering, University of Houston, Houston, TX, USA

^d Nanjing Hydraulic Research Institute, Nanjing 210000, China

HIGHLIGHTS

- The cracking position and failure locations can be identified.
- The load level corresponding to the occurrence of major cracks can be captured accurately.
- The amplitude of focused signals can accurately present the stiffness degradation of BFRP reinforced concrete structures.
- The deflection can be accurately predicted based on the amplitude of focused signal.
- The SA transducer is feasible for monitoring the damage status of concrete bending structures.

GRAPHICAL ABSTRACT



ARTICLE INFO

Article history:

Received 21 January 2019

Received in revised form 8 April 2019

Accepted 6 June 2019

Available online 24 June 2019

Keywords:

Basalt fiber reinforced polymer (BFRP) bars

Smart aggregate (SA) transducers

Time reversal method

Structural damage mechanism

ABSTRACT

Fiber reinforced polymer (FRP) bars, as alternatives of steel bars, are encouraged to be utilized in concrete construction due to the properties of both corrosion resistance and high tensile strength. In this paper, smart aggregate (SA) transducers, which can be used as both actuator and sensor, are employed to identify the structural damage mechanism of basalt-FRP (BFRP) bars reinforced concrete beams. Time reversal method is adopted for increasing the signal-to-noise ratio (SNR), which is aimed at obtaining clear amplitude of focused signal. Those methodologies are applied to conduct a further study of the structural mechanism of BFRP reinforced concrete flexural components. The experimental results reveal that the cracking and failure position of the concrete beam reinforced with BFRP bars can be located and the corresponding loads can be identified according to signal change when different crack appears. The stiffness degradation of BFRP bars reinforced concrete beams can be effectively expressed and the deflection can be accurately predicted by acquiring amplitude of focused signals in the overall zone. Additionally, it has been recognized that the damage process and mechanism of BFRP reinforced concrete beams can be accurately evaluated using those SA transducers and the status of those structural components also can be monitored effectively.

© 2019 Elsevier Ltd. All rights reserved.

* Corresponding author.

E-mail addresses: lingzhu_zhou@163.com (L. Zhou), zhengy@dgut.edu.cn (Y. Zheng), gsong@uh.edu (G. Song), chendongdlut@mail.dlut.edu.cn (D. Chen), 15951979677@163.com (Y. Ye).

1. Introduction

It is well-founded that the corrosion of steel reinforcement and fatigue damage lead to degradation of concrete structural performance [1–4]. Therefore, the reduced durability and shortened service life are exposed in this structural component [5]. For existing damaged structures, the repair using fiber reinforced polymer (FRP) materials in the form of fabrics and laminates can retrofit these corrosion-damaged and fatigue-damaged concrete structural [6–11]. In the new-built structures, a new-type of reinforcement, FRP bar, as a substitute for steel bar is encouraged to use in concrete structures owing to its advantages of excellent mechanical properties and corrosion resistance properties [12–16]. Some concrete bridge structures have been constructed with FRP bars, such as the Thompson's Bridge, Mackinleyville Bridge and Talyor Bridge [17]. Zheng et al. [15,18] revealed that basalt-FRP (BFRP) reinforced self-compacting concrete (SCC) deck slabs exhibited good structural behaviors within the service load. Ehab El-Salakawy et al. [19] conducted a field investigation on the bridge deck slab reinforced with glass-FRP (GFRP) bars constructed in Canada, and results revealed that GFRP rebar provided very competitive performance in comparison to steel under actual service conditions.

Due to the properties of FRP materials including low elastic modulus and without yield point, bending members of FRP reinforced concrete have low initial stiffness, large deflection, large crack width and higher possibility of brittle fracture under the same conditions [17]. Mahroug et al. [20] showed that continuous concrete slabs reinforced with BFRP bars had greater deflection and crack width than corresponding steel-reinforced structures. Capozucca [21] conducted a bending test on concrete beam grid reinforced with CFRP bars, and results showed that the key factors in the design of carbon-FRP (CFRP) reinforced concrete beams were the deflection and the crack width. Wegian et al. [22] revealed that the ACI 440 design specification seriously underestimated the shear capacity of FRP reinforced concrete beams. Zhou [17] showed that a series of stiffness degradation models and crack width calculation models of FRP reinforced concrete bending members had significant limitations due to inhomogeneous in structural component. The deflection and crack width are the key factors affecting the normal service of FRP bars reinforced concrete bending members. However, the existing research methods on concrete bending members reinforced with FRP are traditional currently, and the deflection and crack width calculation formula of concrete bending members with FRP bars are semi-empirical, which is based on the modification of the corresponding reinforced concrete members.

The BFRP reinforced self-compacting concrete deck slabs in Thompson Bridge, a real bridge, exhibited similar or better structural behaviors than that of steel within the service load [12,18]. However, the structural deterioration mechanism and design methods of BFRP reinforced concrete bending members have not been fully investigated. In addition, the complexity of mechanical mechanism and the dispersion of materials restrict the development of the design theory of BFRP bars reinforced concrete bending members. Therefore, it is essential to further identify the mechanical mechanism of BFRP bars reinforced concrete bending members using novel technologies, with the aim to promote the use of BFRP bars in actual structure.

Due to their advantages, such as fast response [23–25], strong piezoelectric effect [26], high sensitivity [27,28], wide bandwidth [26], energy harvesting [29], low cost [30] and the dual actuating and sensing function [31], piezoceramic transducers have been widely used in the emerging field of structural health monitoring (SHM) [32–36] and damage detection [37,38]. It is worthwhile to point out that with the dual actuating and sensing function in a wide bandwidth, piezoceramic transducers are often used to generate and detect acoustic waves, stress waves, and ultrasonic

waves that can propagate in many mediums for SHM and nondestructive testing (NDT) [39–41].

Nowadays, piezoceramic enabled active sensing method, which employs at least two transducers with one as an actuator to generate stress waves and the other one as a sensor to detect the propagating waves, has received much attention for SHM of different types of the host structures, including concrete structures [42,43], bolted connections [44], space structures [45], underground structures [46,47] and timber structures [48], among others. In the piezoceramic materials family, Lead Zirconate Titanate (PZT) has a strong piezoelectric effect and is the most commonly used piezoceramic material. PZT is available in a variety of shapes and dimensions, and can be easily packaged for field deployment as embedded or surface-bonded transducers. Song et al. [49] embedded PZT patches in the concrete structure to detect possible cracks. Xu et al. [50,51] detected the debonding damage between concrete and steel tubes in circular concrete-filled steel tubes (CFST) integrated with piezoceramic patches. Taghavi-pour et al. [52] demonstrated that the cracking status of reinforced concrete beams could be evaluated in terms of the peak of power spectral density and damage indexes. A PZT sensor array measurement approach for localizing cracks in concrete structures was proposed by Narayanan et al and the stress wave transmission measurements were performed by using the PZT patches as actuator-receiver (AR) pairs [53]. However, research has rarely been conducted to investigate the failure mechanism and stiffness degradation of bending members reinforced with BFRP bars by using piezoceramic transducers.

The aim of this paper is focused to evaluate the damage status of BFRP reinforced concrete beams from loading to failure by using smart aggregate (SA) transducers based active sensing approach. The time reversal method was adopted to improve the signal-to-noise ratio (SNR) in this experiment. The amplitude of focused signal obtained by the time reversal operation was used to evaluate the cracking state, the degree of stiffness degradation and the location of the failure of the concrete beam reinforced with BFRP bars. The experimental test results show that it is feasible to identify the cracking state, location of the failure and the stiffness degradation degree of the concrete beams by using SA transducers based on the time reversal method. Finally, the deflection of the concrete beams is calculated by the amplitude of focused signals analytically, which agrees well with experimental results.

2. Principle of monitoring flexural behavior of beams using SA transducer based on time reversal method

Time reversal technology was first proposed by Fink [54] in 1992. It is a time domain reverse operation for the received signals and has two properties, namely temporal focusing and spatial focusing [30]. The two properties enable the time reversal technology applicable to the complex environment with severe scattering. The concrete structure is of materials with severe scattering. With the help of the time reversal technology approach, the SNR can be effectively improved. In addition, with its dual sensing and actuating functions, a PZT transducer is almost a perfect time reversal mirror to detect the wave and to re-emit the time-reversed wave [55–57].

Fig. 1 demonstrate the detailed process of time reverse of concrete beam in healthy and damaged state. Four SAs are bonded onto the surface of concrete beam. Taking SA1 and SA3 as an example, the time reversal technology can be list as following: (1) The modulated Guass signal is applied to SA1 to actuate stress waves; (2) SA3 receives the signal of stress waves propagated through the surface of the concrete beam; (3) the received signal is reversed in time domain and the reversed signal is applied to SA3 to re-actuate

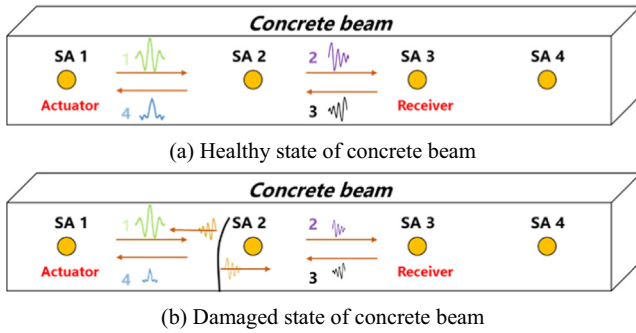


Fig. 1. Principle of time reversal technology.

the stress wave; (4) SA1 receives the reversed signal, which is a focused signal. As shown in Fig. 1(b), a part of the stress waves energy is dissipated during the propagation process when the concrete beam is in a damaged state (the crack is generated). The amount of stress waves energy dissipated is related to the damage levels of concrete beams. Using the time reversal technology, more stress waves energy is dissipated due to stress waves propagating the surface of the concrete beam twice, which means the amplitude of focused signal will be significantly reduced. Hence, the amplitude of focused signal can be used to identify the structural damage mechanism of concrete beam.

3. Experimental setup and procedure

3.1. Materials test and mechanical properties

The materials used in this research were commercial ready-mixed concrete, BFRP bars with diameter of 12 mm and round steel bars with diameter of 6 mm. The mechanical properties tests of commercial ready-mixed concrete were carried out, including cube compressive strength test, axial compressive strength test, elastic modulus test and splitting tensile strength test. As shown in Fig. 2, the tensile tests of reinforcing bars (BFRP bars and round

steel bars) were conducted to obtain tensile strength and elastic modulus.

The test results of mechanical properties of commercial ready-mixed concrete are listed in Table 1, and the properties of reinforcing bars used in this experimental are shown in Table 2.

3.2. Specimens design and fabrication

Two identical concrete beams (B1 and B2) using BFRP bars as longitudinal rebar and round steel bars as transverse rebar were designed. The two concrete beams had a constant cross-section of 150 × 250 mm and a length of 2000 mm. Two BFRP bars with a diameter of 12 mm as longitudinal reinforcement were located at the bottom layer of concrete beams, and two identical BFRP bars as constructional reinforcement were placed on the top layer of concrete beams. Round steel bars with a diameter of 6 mm as stirrup were arranged on the bending-shear section of the concrete beams, and the space between the two stirrups was 150 mm. The longitudinal reinforcement ratio and the stirrup reinforcement ratio were 0.708% and 0.251%, respectively. The cover thickness of the concrete beams and the distance from the center of the section of BFRP bar to the external beam surface were 25 mm and 31 mm in this test. The details of the dimensions and the reinforcement layout are shown in Fig. 3.

The concrete beams were vibrated during casting to eliminate air bubbles. Side molds of the concrete beams were demolished after 1 day, and the surface of concrete beams was covered by wet sponges for curing.

3.3. Transducer arrangement and loading procedure

A smart aggregate, as shown in Fig. 4(a), is made up of two marble blocks and a PZT patch sandwiched embedded between the marble blocks, and the marble blocks have both waterproof and protective effects to avoid physical damage of PZT. Owing to the piezoelectric effect of the PZT, a SA transducer can function as an actuator or a sensor. Four SA transducers were bonded to the outer surface of concrete beam with the aim to identify the failure mech-

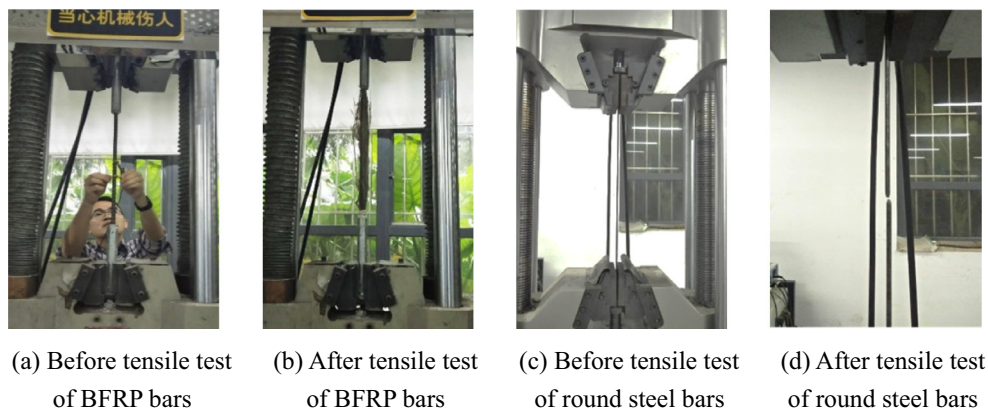


Fig. 2. The tensile tests of BFRP bars and round steel bars.

Table 1
The test results of mechanical properties of commercial ready-mixed concrete.

Mechanical properties	1 day	3 days	7 days	28 days
Cube compressive strength (MPa)	42.5	60.4	67.5	70.1
Axial compressive strength (MPa)	33	48.6	52.7	55.5
Elastic modulus (MPa)	31308.8	33220.1	35380.4	39715.7
Splitting tensile strength (MPa)	3.3	4.7	5.2	5.1

Table 2
The properties of reinforcing bars.

Type	Yield strength (MPa)	Ultimate strength (MPa)	Elastic modulus (MPa)
BFRP Bars	–	1115.3	48,976
Round steel bars	444.3	483.2	–

anism of BFRP bars reinforced concrete beam under four-point bending. Fig. 4(c) depicts the arrangement of SA transducers in detail. In this experiment, the SA1 and SA3 transducers worked as actuators and the SA2 and SA4 transducers worked as sensors. This actuator-sensor layout is used to monitor the damage of concrete beam in the bend-shear zone, the pure bending zone and the overall zone. An active sensing approach [52,58] was used in this research. The instrumentation setup of SA transducers is illustrated in Fig. 4(b), and the device (NI USB 6366) of data acquisition was

employed to generate or receive the signals and a power amplifier was adopted to amplify the emitted signals. In the test, the sampling frequency and the voltage amplitude were 1 MHz and 3 V [59].

As shown in Fig. 5, displacement transducers were placed in the mid-span of concrete beam and the midpoint between the support and mid-span for measuring the vertical deflection. Concrete beams were loaded up to failure under a monotonic load by using an accurately calibrated hydraulic actuator with a capacity of 1000 kN. Before the formal load test, the preloading procedure was performed with 5 kN increments to 10 kN, which was to ensure good contact between the loading device and the surface of concrete beam. However, in the formal load test, the concrete beams were loaded in 10 kN increments until the failure load was reached. The deflections, crack patterns and piezoelectric signals were measured at each step. The loading configuration of concrete beam in this test is given in Fig. 5.

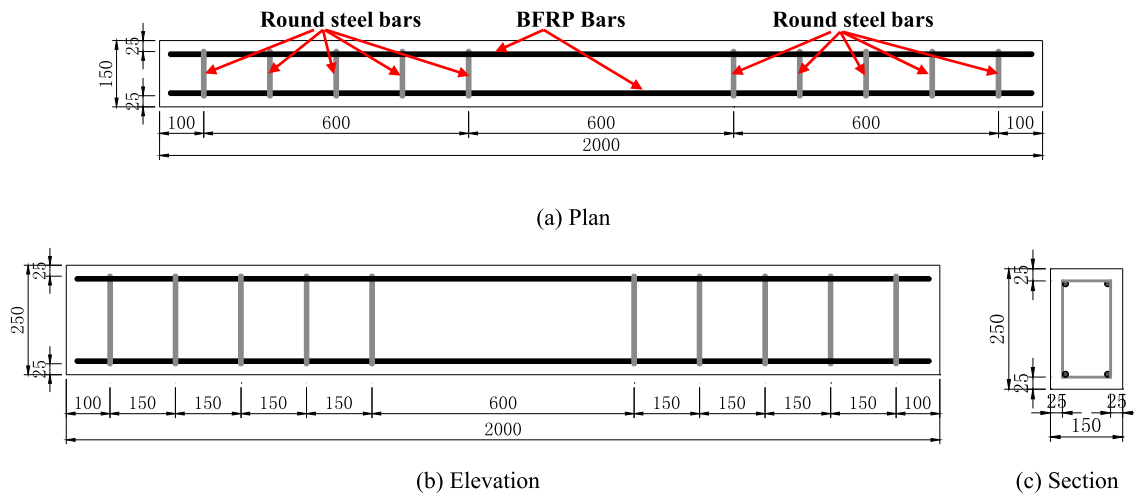


Fig. 3. Reinforcement layout of concrete beams.

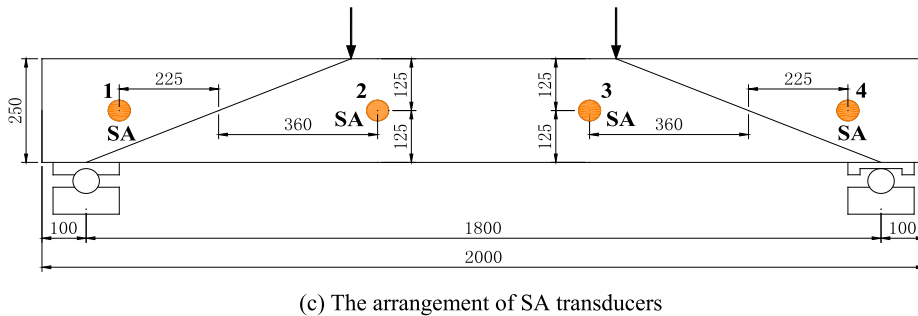
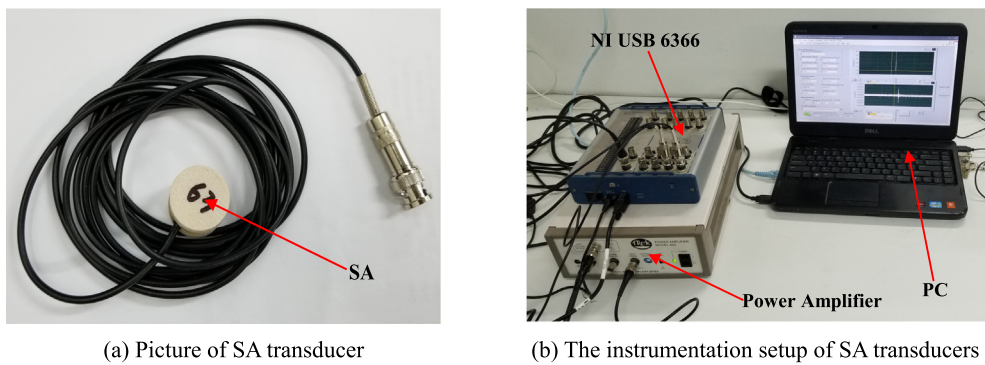


Fig. 4. The instrumentation setup and the arrangement of SA transducers.

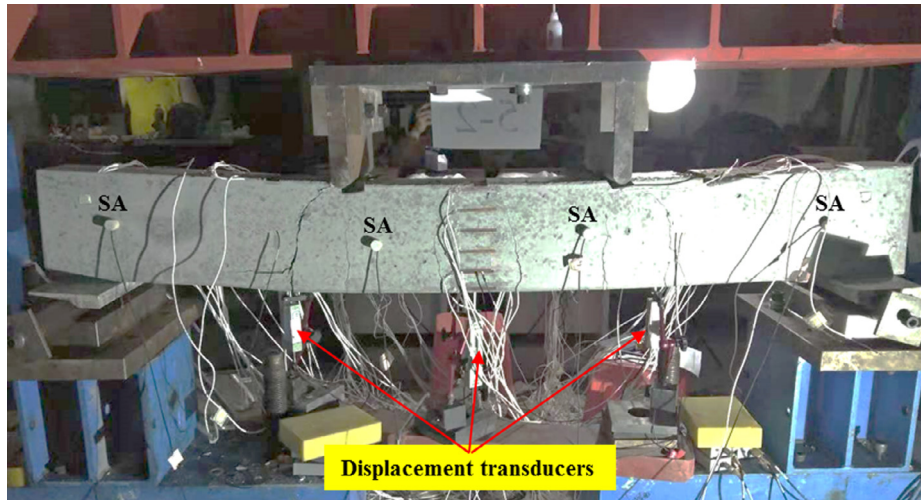


Fig. 5. Loading configuration of concrete beam in this test.

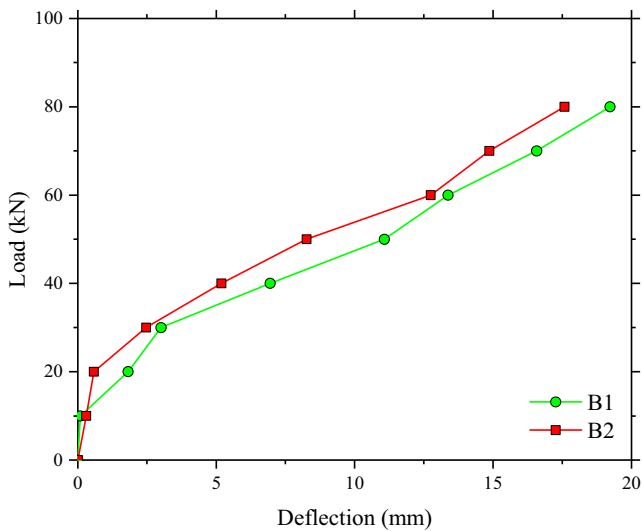
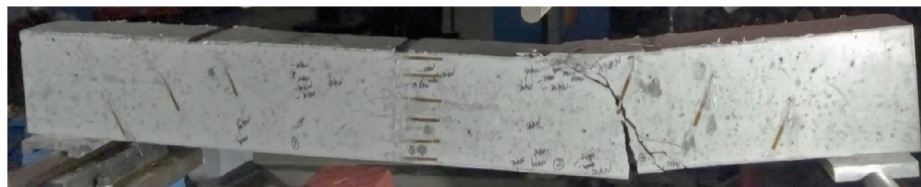


Fig. 6. Load-deflection curves of concrete beams.

4. Experimental results discussion

4.1. Ultimate bearing capacity and failure mode of concrete beams

The ultimate bearing capacities for the B1 and B2 concrete beams reinforced with BFRP bars were 97 kN and 100.7 kN, respectively, and the cracking loads of those two specimens were both 20 kN. It is worth noting that the load-deflection curves after 80kN are not plotted because the deflection varies greatly during the process of data acquisition when the concrete beams are approaching failure. The load-deflection responses of the tested beams are shown in Fig. 6. It can be observed that the curves are approximately bilinear, which is attributed to the linear elastic constitutive of BFRP bars. A linear behavior is revealed in the uncracking stage, while a significantly reduced stiffness is presented after the cracking of the concrete beam. This means that the occurrence of crack leads to a reduction of effective moment of inertia and a decrease of structural behavior. As shown in Fig. 6, the curves of load-deflection are not smooth because of fewer collecting points and longer load-holding time. Failure patterns of concrete beam are shown in Fig. 7, and finally, all concrete beams present shear-compression failure modes.



(a) Concrete beam B1



(b) Concrete beam B2

Fig. 7. Failure patterns of concrete beam.

4.2. Monitoring results using SAs

The piezoelectric signals in Sections 1-2, 2-3, 3-4 and 1-4 were measured upon emitting signals using the SA1 and SA3 as actuators and receiving signals using the SA2 and SA4 as sensors. The amplitude of focused signals acquired from SA transducers corresponding to the Sections 1-2, 2-3, 3-4 and 1-4 are plotted in Fig. 8, and the three stages during the loading of the concrete beams reinforced with BFRP bars are clearly seen: (a) uncracking stage; (b) cracking stage; (c) crack propagation and failure stage. In the uncracking stage, it can be found that the amplitude of focused signals barely changes, which means that the concrete beams are substantially free of damage in the uncracking stage. However, the curves in Section 1-4 clearly show that there is a drastic decline of the amplitude in the cracking stage of concrete

beams. Due to the lower elasticity modulus of BFRP bars and the poor bonding properties between BFRP bars and concrete, the cracks of large and long are occurred (see Fig. 9) when the tensile strain at the bottom of concrete beam is greater than the ultimate tensile strain [17]. Therefore, the amplitude of the wave and the transmission energy in Section 1-4 decrease sharply due to the existence of cracks, which implies that the reduced amplitude is correlated with the damage degree of concrete beams reinforced with BFRP bars [58]. In the crack propagation and failure stage, the amplitude in Section 1-4 has a subtle change with the increase of the load. This can be explained by the fact that large area cracks of concrete beams reinforced with BFRP bars lead to amplitude of the wave and the transmission energy to be completely dissipated.

It can be observed in Fig. 9(a) that the first and second cracks appear respectively in Sections 3-4 and 1-2 of concrete beam rein-

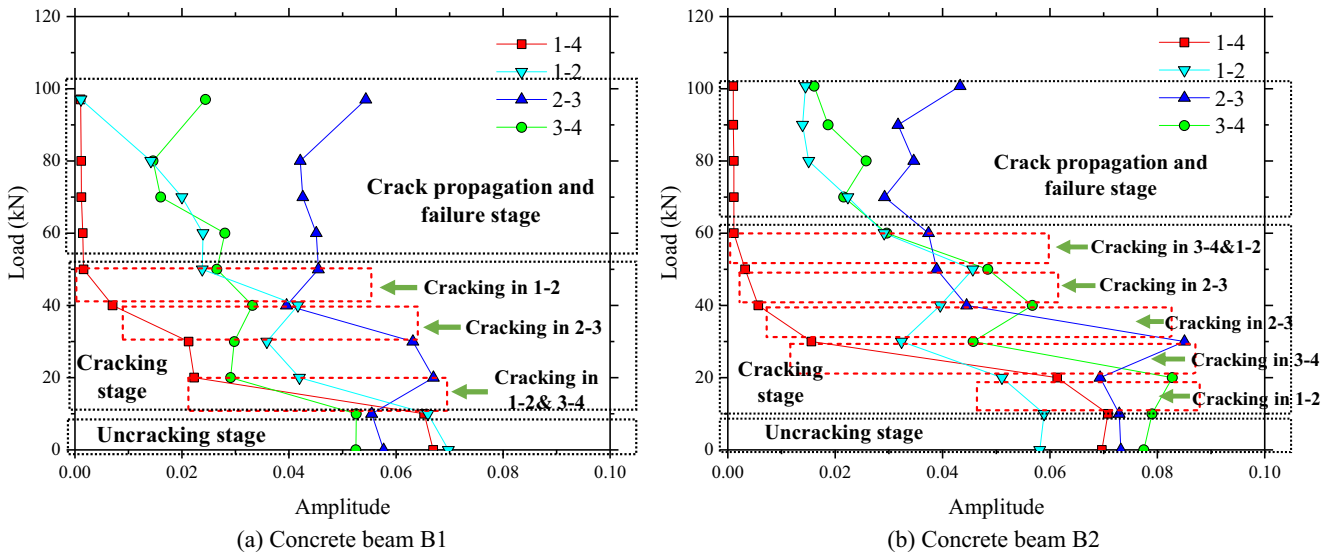


Fig. 8. Amplitude of different focused signals in time reverse method.

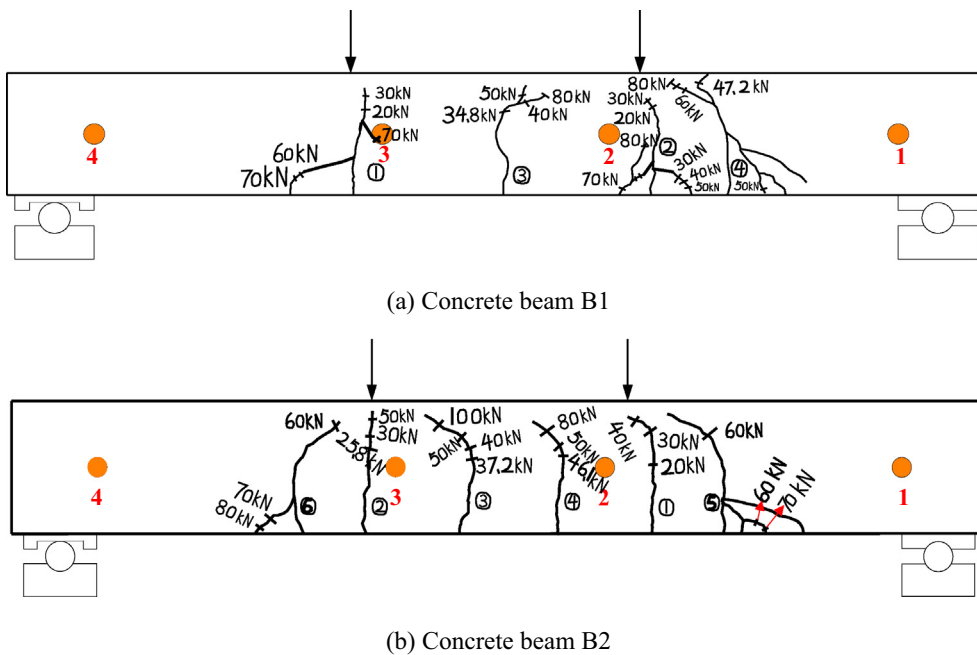


Fig. 9. Cracking patterns of concrete beam.

forced with BFRP bars when the load is 20 kN. Correspondingly, the amplitude of focused signals in Sections 3–4 and 1–2 reduce rapidly, while the amplitude in Section 2–3 increases, as shown in Fig. 8(a). Since the concrete stress is released at the location of cracking when the concrete beam occurs crack and it leads to the reduction of average stress of concrete on both sides of the crack [60]. The third crack occurs in Section 2–3 when the load is 34.8 kN. Similarly, the amplitude in Section 2–3 decreases significantly and in Sections 1–2 and 3–4 increase slightly. When the load is 50 kN, the last crack for concrete beam B1 appears in Section 1–2, and the amplitude in Section 1–2 reduces markedly and that in Section 2–3 increases marginally. While the amplitude in Section 3–4 decreases, which may indicate that the crack in Section 3–4 has a large crack development. The amplitude in Section 1–2 is still decreasing when the load exceeds 50 kN, which means the crack in Section 1–2 continues to propagate until crack through cross-section and finally causes the failure of the concrete beam. This is consistent with the results in Fig. 7(a). In summary, it is feasible to capture the load that appears for each crack and identify the cracking and failure position of the concrete beam reinforced

with BFRP bars by obtaining the signal amplitude from SA transducers. For concrete beam B2, the similar results can be found in Fig. 8(b) and Fig. 9(b).

The results, based on the time reversal method, in Section 1–4 for concrete beam reinforced with BFRP bars (B2) at the load of 0 kN, 40 kN and 80 kN are shown in Figs. 10, 15, and 16, respectively. As shown in Fig. 10(b) and Fig. 11(b), the amplitude of the received signal can be clearly seen at load of 0 kN, while the amplitude of the received signal cannot be completely identified at load of 40 kN due to the noise. This indicates that increasing the applied load results in reduction of the amplitude of the received signal and it can lead to the loss of information because the amplitude is covered by the noise. The focused signal in Fig. 10(d) and Fig. 11(d), as result of the time reversal technique, presents a distinct peak and higher SNR, which is beneficial to obtain detailed information about structural damage of concrete beam reinforced with BFRP bars [61]. As shown in Fig. 12(d), the amplitude of focused signal is nearly vanished when the beams are in the crack propagation and failure stage. Since transmission energy is severely obstructed owing to the presence of large cracks.

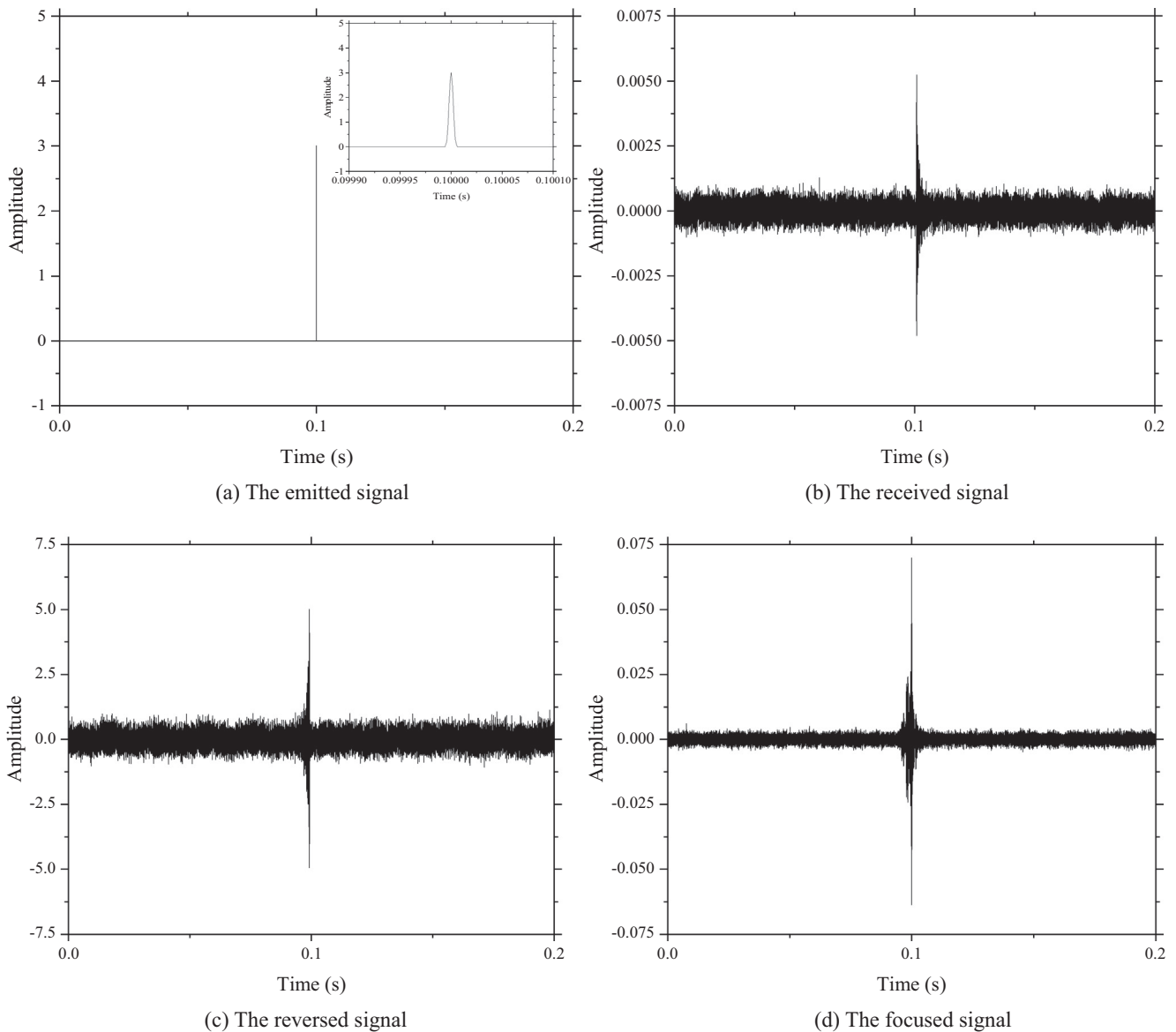


Fig. 10. Four different signals in Section 1–4 at load of 0 kN for the concrete beam B2.

4.3. Comparison and verification

The relationships of load versus deflection and regularization amplitude are shown in Fig. 13, where the regularization amplitude refers to the normalization of the amplitude of focused signals in Section 1–4 of concrete beams reinforced with BFRP bars. In the uncracking stage, the smaller deflection of the concrete beam is revealed due to the integrated stiffness. At the cracking stage, the regularization amplitude drops sharply, the stiffness of the concrete beams degrades significantly and the deflection increases rapidly. This implies that the development of cracks results in the damage evolution of concrete beam reinforced with BFRP bars. The deflection during the cracking phase may exceed the design deflection limit ($\Delta = L/250 = 7.2$ mm) for normal service of concrete beam reinforced with BFRP bars [62,63], which indicates that the design deflection limit has sufficient surplus coefficient to ensure the safety of those structure components. In the crack propagation and failure stage, the deflection of the concrete beam increases greatly with the increasing load.

The theoretical models of effective moment of inertia are shown in Table 3 and the curves of effective moment of inertia of concrete beam reinforced with BFRP bars are revealed in Fig. 14, respectively [64–69]. The comparison of curves between the regularization effective stiffness and the regularization amplitude is presented in Fig. 15. It can be found that the curves of regularization amplitude are similar to the regularization effective stiffness, which implies that amplitude of focused signals in Section 1–4 of concrete beams can substantially reflect the stiffness degradation and the damage level of the structure. As shown in Fig. 15, the cracking load is slightly overestimated by using the theoretical formula. While the regularization effective stiffness of transformed cracked section is higher than the regularization amplitude when the load exceeds 50kN, which is attributed to the amplitude of focused signals are nearly vanished in the crack propagation and failure stage of concrete beams. The regularization amplitude by SA transducers received significantly underestimates the regularization effective stiffness of the reinforced concrete beams in the crack propagation and failure stage. This means that incorrect or

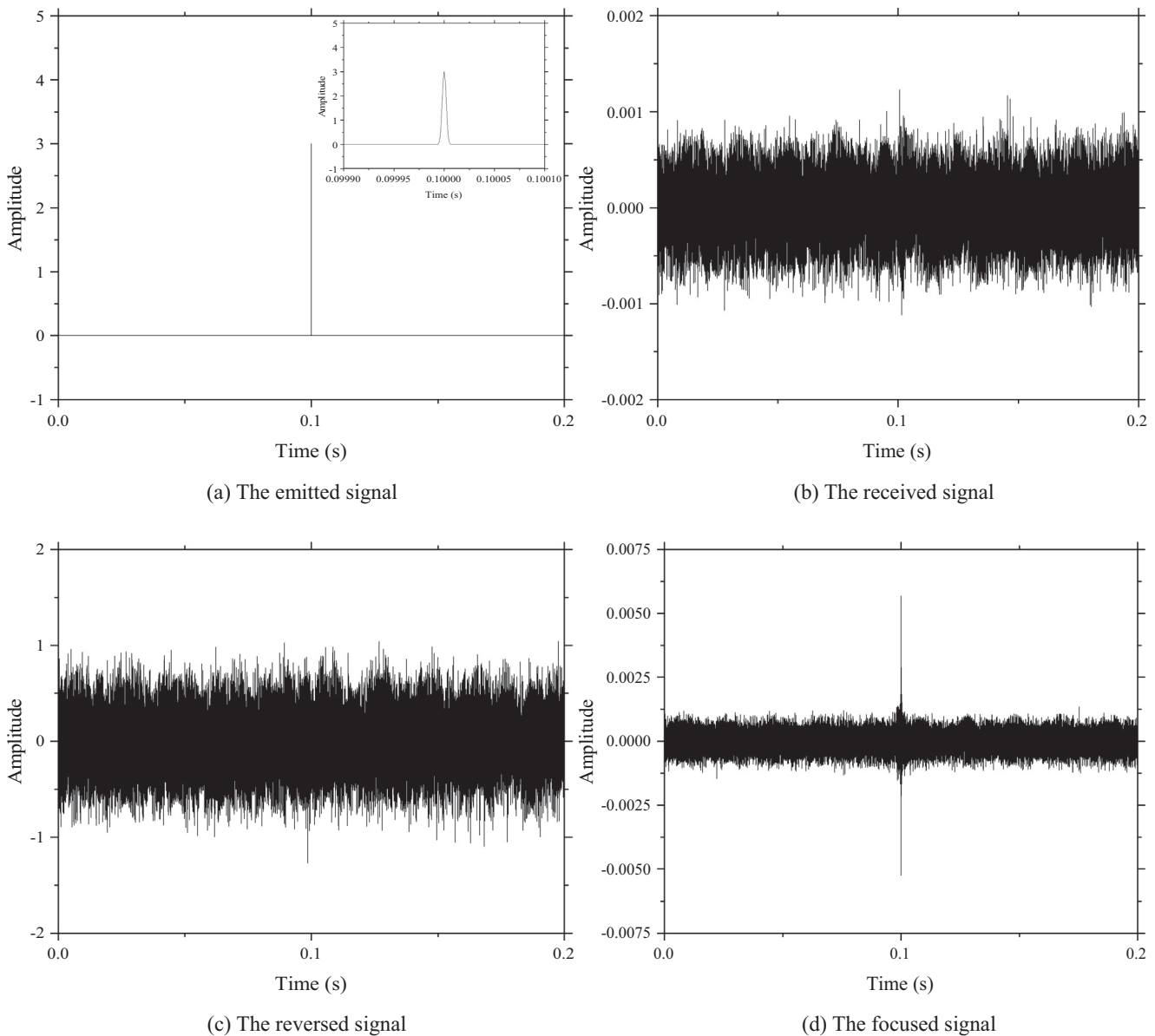


Fig. 11. Four different signals in Section 1–4 at load of 40 kN for the concrete beam B2.

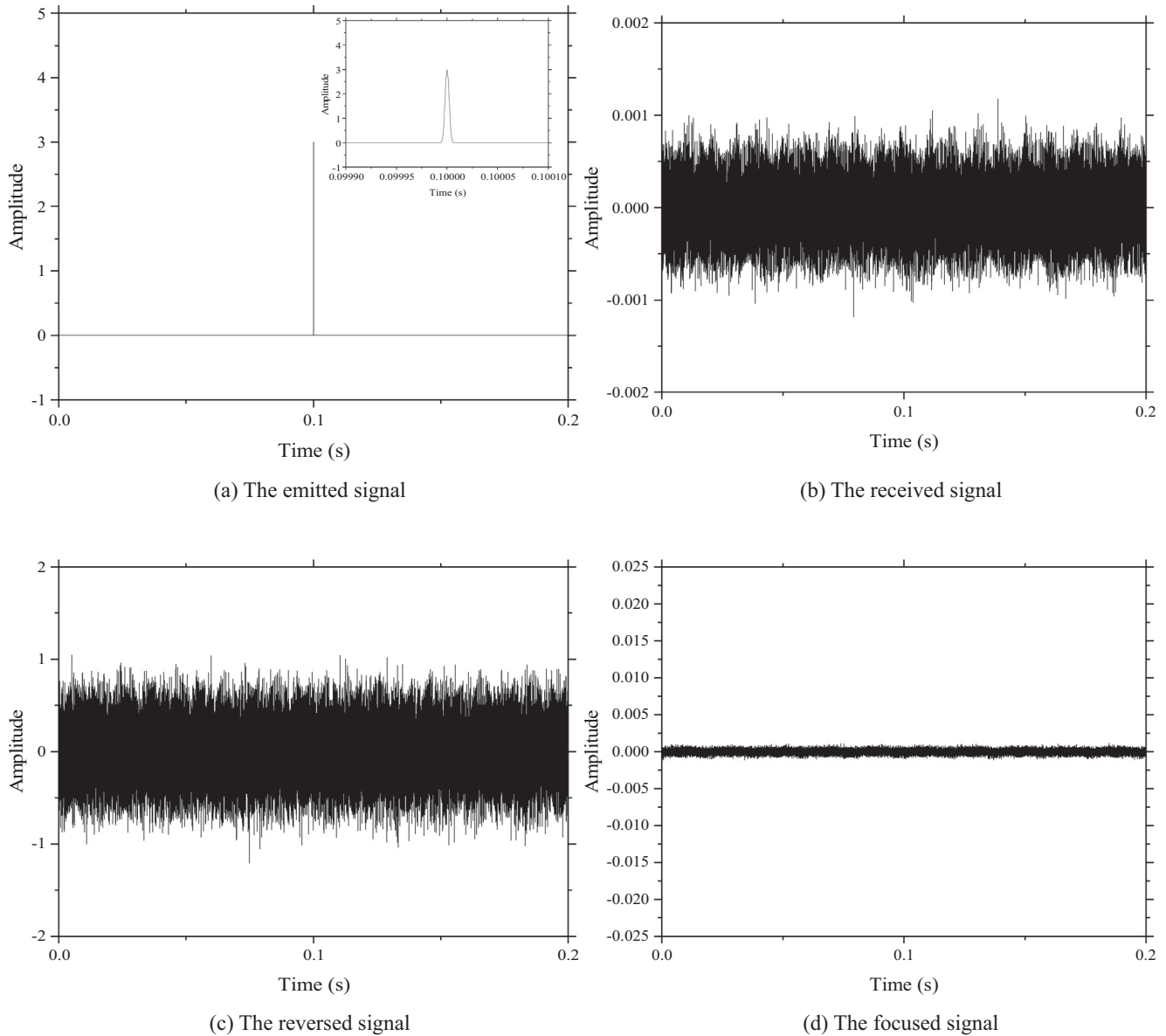


Fig. 12. Four different signals in Section 1–4 at load of 80 kN for the concrete beam B2.

inaccurate information may be generated by receiving focused signals when the reinforced concrete beams are in crack propagation and failure stage. Therefore, further improvement of the monitoring method of SA transducer is necessary.

The calculation formula of the mid-span deflection of the four-point loading of the simply supported member is as follows:

$$\delta_{\max} = \frac{Fa}{24E_c I_e} (3L^2 - 4a^2) \quad (1)$$

where F and a represent the support reacting force and the distance from the loading point to the support, respectively. The comparison of experimental results and theoretical calculation results of load-deflection of concrete beam is illustrated in Fig. 16. The load-deflection curves of SA-B1 and SA-B2 are calculated by adopting the regularization amplitude of focused signals in Section 1–4 of concrete beams respectively, as shown in Fig. 15. However, the effective stiffness of transformed cracked section instead of the amplitude of focused signals is used for the deflection calculation when the regularization amplitude is less than regularization effective stiffness in the later stage. Since the regularization amplitude

significantly underestimates the regularization effective stiffness in the crack propagation and failure stage. As shown in Fig. 16, the load-deflection curves of SA-B1 and SA-B2 agree well with the load-deflection curves of the experiment. This indicates that SA transducers are feasible for monitoring damage and predicting deformation of concrete beam with BFRP reinforced. The load-deflection curves between prediction based on SA transducers and the experiment have a small error in the cracking stage, which may be attributed to the incomplete synchronization of signal data acquisition and deflection data acquisition.

5. Discussion

Considering those SAs, which are larger in size than concrete coarse aggregates, embedded in concrete affects the crack pattern of the concrete beam, the method of SA transducers bonded to the surface of concrete beam is adopted in this experiment. While this method whether is equivalent to SA embedded in concrete is worth explored. The collected data curves were not smooth in

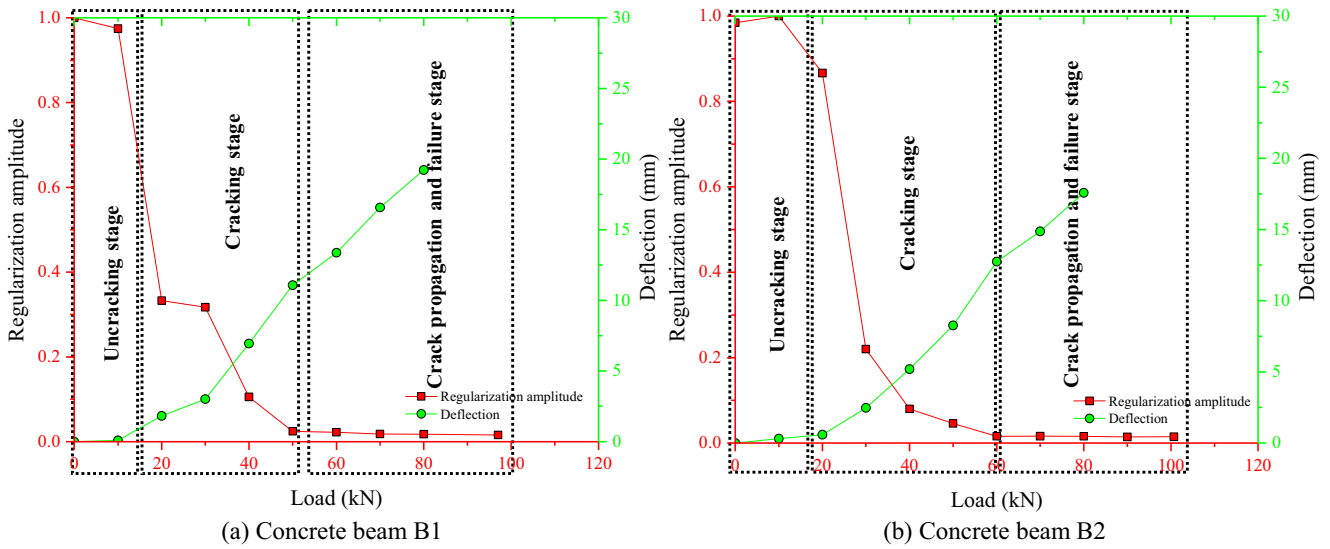


Fig. 13. Load vs deflection and regularization amplitude.

Table 3
Theoretical models of effective moment of inertia.

Theoretical model	Equation	
ACI 318-05 [64]	$I_e = \left(\frac{M_{cr}}{M_a}\right)^3 I_g + \left[1 - \left(\frac{M_{cr}}{M_a}\right)^3\right] I_{cr} \leq I_g$	Eq. (1)
ACI 440.1R-03 [65]	$I_e = \left(\frac{M_{cr}}{M_a}\right)^3 \beta_d I_g + \left[1 - \left(\frac{M_{cr}}{M_a}\right)^3\right] I_{cr} \leq I_g$ $\beta_d = \alpha_b \left[\frac{E_f}{E_s} + 1\right] \alpha_b = 0.5$	Eq. (2)
ACI 440.1R-06 [66]	$I_e = \left(\frac{M_{cr}}{M_a}\right)^3 \beta_d I_g + \left[1 - \left(\frac{M_{cr}}{M_a}\right)^3\right] I_{cr} \leq I_g \quad \beta_d = \frac{1}{5} \left(\frac{\rho_f}{\rho_{fb}}\right)$	Eq. (3)
Benmokrane [67]	$I_e = \frac{1}{\beta} \left(\frac{M_{cr}}{M_a}\right)^3 I_g + \alpha \left[1 - \left(\frac{M_{cr}}{M_a}\right)^3\right] I_{cr} \leq I_g$ $\beta = 7.0 \quad \alpha = 0.84$	Eq. (4)
ACI 440.1R-15 [68]	$I_e = \frac{I_{cr}}{1 - \gamma \left(\frac{M_{cr}}{M_a}\right)^2 \left(1 - \frac{I_{cr}}{I_g}\right)} \leq I_g$ $\gamma = 1.72 - 0.72 \left(\frac{M_{cr}}{M_a}\right)$	Eq. (5)
ISIS Canada [69]	$I_e = \frac{I_g I_{cr}}{I_g + \left[1 - 0.5 \left(\frac{M_{cr}}{M_a}\right)^2\right] (I_g - I_{cr})}$	Eq. (6)
Faza and Gangarao [64]	$\delta = \frac{23P^2}{648E_c I_m} \quad I_m = \frac{23I_g I_{cr}}{8I_{cr} + 13I_g} \quad I_e = ACI (I_e)$	Eq. (7)

Note: I_e – Effective moment of inertia; I_g – Gross moment of inertia; I_{cr} – Moment of inertia of transformed cracked section; M_{cr} – Cracking moment; M_a – Applied moment; E_f – Elastic modulus of FRP; E_s – Elastic modulus of steel; E_c – Elastic modulus of concrete; ρ_f – Reinforcement ratio of FRP; ρ_{fb} – Reinforcement ratio of FRP producing balanced strain conditions; L – Span length of member; P – Applied load.

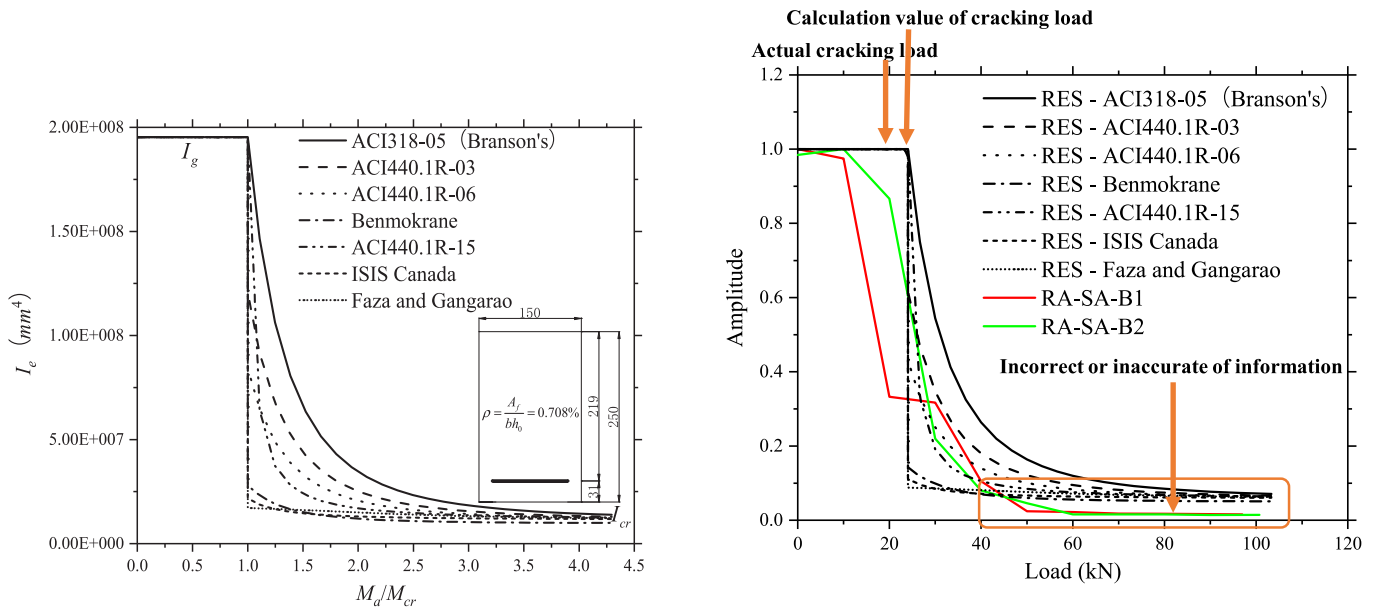


Fig. 14. The curves of effective moment of inertia.

Fig. 15. Comparison of the curves between the regularization effective stiffness (RES) and the regularization amplitude (RA).

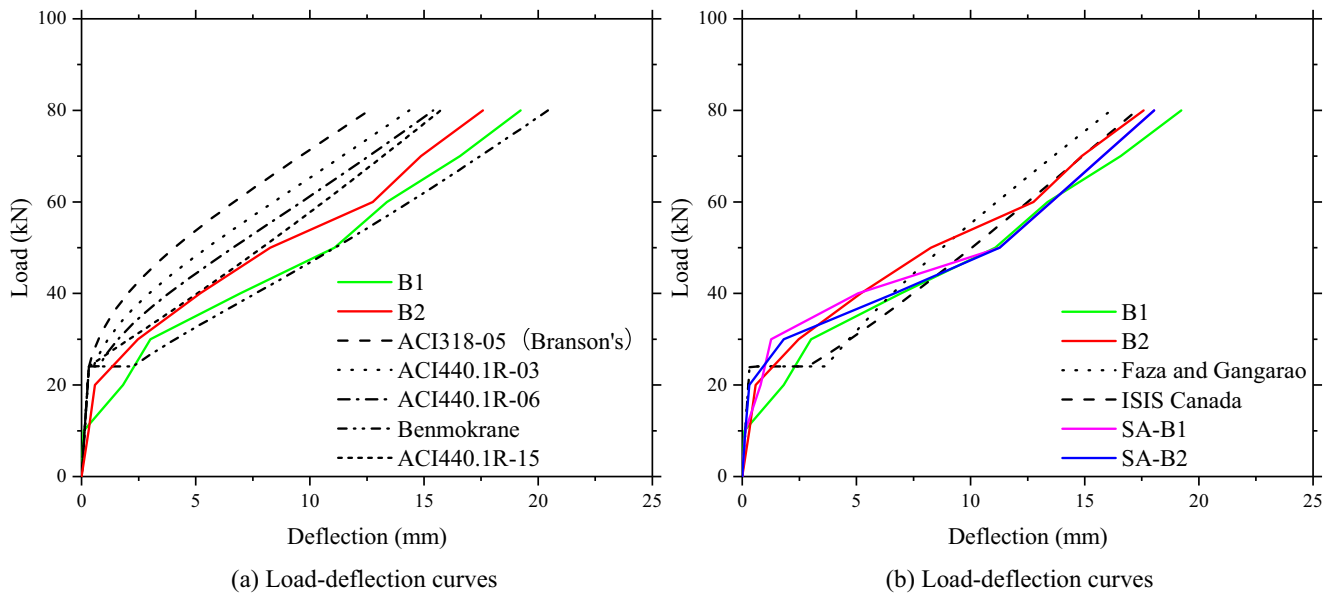


Fig. 16. Comparison of experimental results and theoretical calculation results of load-deflection of concrete beams.

the experiment and the structural damage cannot be accurately identified by SAs transducers, which was caused by the loading method and acquisition method. Therefore, it is significant to achieve dynamic synchronous acquisition of all data during continuous loading. SA transducers received the regularization amplitude of focused signal significantly underestimates the regularization effective stiffness of reinforced concrete beam in the crack propagation and failure stage. In the future, further research on the damage of concrete beam based on SA will be carried out and the new monitoring methods based on SA could open a possibility of solving the problem of the amplitude of focused signal is nearly vanished in the crack propagation and failure stage of concrete beam. In this test, the crack did not appear in the location of SA transducers, while the crack at the location of SA transducers will directly affect the received signal. Thus, it is meaningful to explore the effect of the crack at the location of SA transducers on the received signal in the future research.

6. Conclusions

In this paper, a series of piezoceramic transducers enabled time reversal method is proposed to identify the structural damage mechanism of BFRP bars reinforced concrete beams. Four SA transducers were bonded to the surface of concrete beam in order to detect its damage in the bend-shear zone, the pure bending zone and the overall zone. Concrete beams reinforced with BFRP bars were divided into three stages during the loading process: (a) uncracking stage; (b) cracking stage; (c) crack propagation and failure stage. Base on the time reversal technique and the experimental results, the main conclusions of this paper are drawn as follows:

- (1) The amplitude of focused signals is barely changed in the uncracking stage of concrete beams, while the amplitude of focused signals changes dramatically in the crack propagation and failure stage of concrete. This is attributed to the existence of cracks that hinders the propagation of the wave, which results in the reduction of amplitude of focus signals.
- (2) According to the variation in the amplitude of focused signals in different sections, the cracking position and failure position of the concrete beam reinforced with BFRP bars can be identified and the load when the major crack appears can be captured.

- (3) The amplitude of focused signals (in the overall zone) can accurately present the stiffness degradation of concrete beams reinforced with BFRP bars.
- (4) The deflection calculated from the amplitude of focused signal (in the overall zone) agrees well with experimental results and the SA transducer has the ability to predict deformation of concrete beam with BFRP reinforced.
- (5) The experimental programs successfully demonstrate piezoceramic SA transducer is feasible for evaluating the damage of concrete bending structures reinforced with BFRP bars, and it has the potential for monitoring the health of reinforced concrete bending structures in general.

Author contributions

Yu Zheng and Gangbing Song conceived and designed the experiments; Lingzhu Zhou and Yuxiao Ye performed the experiments; Lingzhu Zhou, Dongdong Chen, Yu Zheng and Gangbing Song analyzed the data; Lingzhu Zhou wrote the paper; Yu Zheng and Gangbing Song revised the paper.

Declaration of Competing Interest

None.

Acknowledgements

This work was supported by the Natural Science Foundation of China (51678149), the Guangdong Science and Technology Planning, China (2016A010103045), the Key Research Project by Department of Education of Guangdong Province, China (2018KZDXM068) and Guangdong Natural Science Foundation, China (2018A030313864). The authors are sincerely grateful for these financial supports.

References

- [1] A. Bossio, T. Monetta, F. Bellucci, G.P. Lignola, A. Prota, Modeling of concrete cracking due to corrosion process of reinforcement bars, *Cem. Concr. Res.* 71 (2015) 78–92.
- [2] J.G. Cabrera, Deterioration of concrete due to reinforcement steel corrosion, *Cem. Concr. Compos.* 18 (1) (1996) 47–59.

- [3] G.G. Triantafyllou, T.C. Rousakis, A.I. Karabinis, Analytical assessment of the bearing capacity of RC beams with corroded steel bars beyond concrete cover cracking, *Compos. B Eng.* 119 (2017) 132–140.
- [4] P.G. Li, C. Andrea, S. Andrea, S. Wei, Experimental and numerical investigations on fatigue damage propagation and life prediction of high-performance concrete containing reactive mineral admixtures, *Int. J. Fatigue* 32 (2) (2010) 227–237.
- [5] L. Chernin, D.V. Val, Prediction of corrosion-induced cover cracking in reinforced concrete structures, *Constr. Build. Mater.* 25 (2011) 1854–1869.
- [6] J.H. Xie, R.L. Hu, Experimental study on rehabilitation of corrosion-damaged reinforced concrete beams with carbon fiber reinforced polymer, *Constr. Build. Mater.* 38 (2) (2013) 708–716.
- [7] G.G. Triantafyllou, T.C. Rousakis, A.I. Karabinis, Effect of patch repair and strengthening with EBR and NSM CFRP laminates for RC beams with low, medium and heavy corrosion, *Compos. B Eng.* 133 (2018) 101–111.
- [8] M. Badawi, K. Soudki, Control of corrosion-induced damage in reinforced concrete beams using carbon fiber-reinforced polymer laminates, *J. Compos. Constr.* 9 (2) (2005) 195–201.
- [9] C. Apa Gheorghiu, Pierre Labossière, J. Proulx, Response of CFRP-strengthened beams under fatigue with different load amplitudes, *Constr. Build. Mater.* 21 (4) (2007) 756–763.
- [10] E. Ferrier, D. Bigaud, J.C. Clément, P. Hamelin, Fatigue-loading effect on rc beams strengthened with externally bonded FRP, *Constr. Build. Mater.* 25 (2) (2011) 539–546.
- [11] B.G. Charalambidi, T.C. Rousakis, A.I. Karabinis, Analysis of the fatigue behavior of reinforced concrete beams strengthened in flexure with fiber reinforced polymer laminates, *Compos. B Eng.* 96 (2016) 69–78.
- [12] L.Z. Zhou, Y. Zheng, S. Taylor, Finite-element investigation of the structural behavior of Basalt Fiber Reinforced Polymer (BFRP) - reinforced Self-Compacting Concrete (SCC) decks slabs in Thompson bridge, *Polymers* 10 (6) (2018) 678.
- [13] Y. Zheng, X.Y. Fu, Z.Y. Lu, Y.F. Pan, Investigation of structural behaviour of GFRP reinforced concrete deck slabs through NLFEA, *Constr. Build. Mater.* 45 (2013) 60–77.
- [14] X.Z. Lu, J.F. Chen, L.P. Ye, J.G. Teng, J.M. Rotter, RC beams shear-strengthened with FRP: stress distributions in the FRP reinforcement, *Constr. Build. Mater.* 23 (4) (2009) 1544–1554.
- [15] Y. Zheng, L.Z. Zhou, L.P. Xia, Y.B. Luo, S. Taylor, Investigation of the behaviour of SCC bridge deck slabs reinforced with BFRP bars under concentrated loads, *Eng. Struct.* 171 (2018) 500–515.
- [16] Y. Zheng, C. Sun, T. Deng, J.B. Yang, Z.Y. Lu, Arching action contribution to punching failure of GFRP-reinforced concrete bridge deck slabs, *Arab. J. Sci. Eng.* 39 (2014) 8609–8625.
- [17] L.Z. Zhou, Research on the Flexural Behavior of Self-compacting Fibre Reinforced Concrete Bridge Deck Slabs with BFRP Bars, South China University of Technology, 2018.
- [18] Y. Zheng, S. Taylor, M. Sonebi, D. Robinson, The influence of arching action on BFRP reinforced SCC deck slabs in the Thompson bridge, in: *Proceedings of the 24th Australasian Conference on the Mechanics of Structures and Materials*, Perth, Australia, 2016, pp. 6–9.
- [19] E. Elsalakawy, B. Benmokrane, A. Elragaby, D. Nadeau, Field investigation on the first bridge deck slab reinforced with glass FRP bars constructed in Canada, *J. Compos. Constr.* 9 (6) (2005) 470–479.
- [20] M.E.M. Mahroug, A.F. Ashour, D. Lam, Experimental response and code modelling of continuous concrete slabs reinforced with BFRP bars, *Compos. Struct.* 107 (1) (2014) 664–674.
- [21] R. Capozucca, Analysis of the experimental flexural behaviour of a concrete beam grid reinforced with C-FRP bars, *Compos. Struct.* 79 (4) (2007) 517–526.
- [22] F.M. Wegian, H.A. Abdalla, Shear capacity of concrete beams reinforced with fiber reinforced polymers, *Compos. Struct.* 71 (1) (2005) 130–138.
- [23] F.R. Wang, L.S. Huo, G.B. Song, A piezoelectric active sensing method for quantitative monitoring of bolt loosening using energy dissipation caused by tangential damping based on the fractal contact theory, *Smart Mater. Struct.* 27 (2017) 015023.
- [24] L. Huo, X. Li, D. Chen, H. Li, G. Song, Identification of the impact direction using the beat signals detected by piezoceramic sensors, *Smart Mater. Struct.* 26 (8) (2017) 085020.
- [25] M. Luo, W. Li, C. Hei, G. Song, Concrete infill monitoring in concrete-filled FRP tubes using a PZT-based ultrasonic time-of-flight method, *Sensors* 16 (12) (2016) 2083.
- [26] K. Xu, Q. Deng, L. Cai, S. Ho, G. Song, Damage detection of a concrete column subject to blast loads using embedded piezoceramic transducers, *Sensors* 18 (5) (2018) 1377.
- [27] F.R. Wang, S.C.M. Ho, L.S. Huo, G.B. Song, A novel fractal contact-electromechanical impedance model for quantitative monitoring of bolted joint looseness, *IEEE Access* 6 (2018) 40212–40220.
- [28] D. Ai, H. Zhu, H. Luo, Sensitivity of embedded active PZT sensor for concrete structural impact damage detection, *Constr. Build. Mater.* 111 (2016) 348–357.
- [29] G. Wang, Analysis of bimorph piezoelectric beam energy harvesters using Timoshenko and Euler-Bernoulli beam theory, *J. Intell. Mater. Syst. Struct.* 24 (2) (2013) 226–239.
- [30] L. Huo, D. Chen, Q. Kong, H. Li, G. Song, Smart washer—a piezoceramic-based transducer to monitor looseness of bolted connection, *Smart Mater. Struct.* 26 (2) (2017) 025033.
- [31] B.N. Agrawal, M.A. Elshafei, G. Song, Adaptive antenna shape control using piezoelectric actuators, *Acta Astronaut.* 40 (11) (1997) 821–826.
- [32] G. Song, C. Wang, B. Wang, Structural Health Monitoring (SHM) of Civil Structures, *Multidisciplinary Digital, Publishing Institute*, 2017.
- [33] V. Memmolo, E. Monaco, N. Boffa, L. Maio, F. Ricci, Guided wave propagation and scattering for structural health monitoring of stiffened composites, *Compos. Struct.* 184 (2018) 568–580.
- [34] D. Wang, Q. Wang, H. Wang, H. Zhu, Experimental study on damage detection in timber specimens based on an electromechanical impedance technique and RMSD-based mahalanobis distance, *Sensors* 16 (10) (2016) 1765.
- [35] L.S. Huo, F.R. Wang, H.N. Li, G.B. Song, A fractal contact theory based model for bolted connection looseness monitoring using piezoceramic transducers, *Smart Mater. Struct.* 26 (2017) 104010.
- [36] Q. Kong, G. Song, A comparative study of the very early age cement hydration monitoring using compressive and shear mode smart aggregates, *IEEE Sens. J.* (2016) 1.
- [37] D. Broda, W.J. Staszewski, A. Martowicz, T. Uhl, V.V. Silberschmidt, Modelling of nonlinear crack-wave interactions for damage detection based on ultrasound—A review, *J. Sound Vib.* 333 (4) (2014) 1097–1118.
- [38] X. Hu, H. Zhu, D. Wang, A study of concrete slab damage detection based on the electromechanical impedance method, *Sensors* 14 (10) (2014) 19897–19909.
- [39] M. Mitra, S. Gopalakrishnan, Guided wave based structural health monitoring: A review, *Smart Mater. Struct.* 25 (5) (2016) 053001.
- [40] Y. Wang, X. Zhu, H. Hao, J. Ou, Guided wave propagation and spectral element method for debonding damage assessment in RC structures, *J. Sound Vib.* 324 (3) (2009) 751–772.
- [41] V.P. Venugopal, G. Wang, Modeling and analysis of lamb wave propagation in a beam under lead zirconate titanate actuation and sensing, *J. Intell. Mater. Syst. Struct.* 26 (13) (2015) 1679–1698.
- [42] W. Liao, J.X. Wang, G. Song, H. Gu, C. Olmi, Y.L. Mo, Structural health monitoring of concrete columns subjected to seismic excitations using piezoceramic-based sensors, *Smart Mater. Struct.* 20 (12) (2011) 125015.
- [43] Q. Kong, R. Robert, P. Silva, Y.L. Mo, Cyclic crack monitoring of a reinforced concrete column under simulated pseudo-dynamic loading using piezoceramic-based smart aggregates, *Appl. Sci.* 6 (11) (2016) 341.
- [44] H. Yin, T. Wang, D. Yang, S. Liu, J. Shao, Y. Li, A smart washer for bolt looseness monitoring based on piezoelectric active sensing method, *Appl. Sci.* 6 (11) (2016) 320.
- [45] J. Xu, C. Wang, H. Li, C. Zhang, J. Hao, S. Fan, Health monitoring of bolted spherical joint connection based on active sensing technique using piezoceramic transducers, *Sensors* 18 (6) (2018) 1727.
- [46] G. Song, W. Li, B. Wang, S.C.M. Ho, A review of rock bolt monitoring using smart sensors, *Sensors* 17 (4) (2017) 776.
- [47] B. Wang, L. Huo, D. Chen, W. Li, G. Song, Impedance-based pre-stress monitoring of rock bolts using a piezoceramic-based smart washer—A feasibility study, *Sensors* 17 (2) (2017) 250.
- [48] J. Zhang, Y. Huang, Y. Zheng, A feasibility study on timber damage detection using piezoceramic-transducer-enabled active sensing, *Sensors* (2018) 1563.
- [49] G. Song, Y. Mo, K. Otero, H. Gu, Health monitoring and rehabilitation of a concrete structure using intelligent materials, *Smart Mater. Struct.* 15 (2) (2006) 309.
- [50] B. Xu, T. Zhang, G. Song, H. Gu, Active interface debonding detection of a concrete-filled steel tube with piezoelectric technologies using wavelet packet analysis, *Mech. Syst. Signal Proc.* 36 (1) (2013) 7–17.
- [51] B. Xu, H. Chen, S. Xia, Numerical study on the mechanism of active interfacial debonding detection for rectangular CFSTs based on wavelet packet analysis with piezoceramics, *Mech. Syst. Signal Proc.* 86 (2017) 108–121.
- [52] S. Taghavipour, S. Kharkovsky, W.H. Kang, B. Samali, O. Mirza, Detection and monitoring of flexural cracks in reinforced concrete beams using mounted smart aggregate transducers, *Smart Mater. Struct.* 26 (10) (2017).
- [53] A. Narayanan, A. Kocherla, K.V. Subramaniam, PZT sensor array for local and distributed measurements of localized cracking in concrete, *Smart Mater. Struct.* (2018).
- [54] M. Fink, Time reversal of ultrasonic fields. i. basic principles, *IEEE Trans. Ultrason. Ferroelectr. Freq. Control* 39 (5) (1992) 555–566.
- [55] G. Du, Q. Kong, F. Wu, J. Ruan, G. Song, An experimental feasibility study of pipeline corrosion pit detection using a piezoceramic time reversal mirror, *Smart Mater. Struct.* 25 (3) (2016) 037002.
- [56] G. Zhang, J. Zhu, Y. Song, C. Peng, G. Song, A time reversal based pipeline leakage localization method with the adjustable resolution, *IEEE Access* (2018) 26993–27000.
- [57] W. Gao, G. Zhang, H. Li, L. Huo, G. Song, A novel time reversal sub-group imaging method with noise suppression for damage detection of plate-like structures, *Struct. Control Health Monitor* 25 (1) (2017).
- [58] G. Song, H. Gu, Y.L. Mo, Smart aggregates: multifunctional sensors for concrete structures—a tutorial and a review, *Smart Mater. Struct.* 17 (2008) 033001.
- [59] T. Zeng, L.S. Huo, W. Gao, H.N. Li, G. Song, Modelling of attenuation of stress wave in concrete based on rayleigh damping model using time-reversal and PZT transducers, *Smart Mater. Struct.* 26 (10) (2017).
- [60] C.B. Peña, Serviceability behaviour of fibre reinforced polymer reinforced concrete beams, *Tdx Tesis Doctorals, En Xarxa* (2011).
- [61] L. Huo, B. Wang, D. Chen, G. Song, Monitoring of pre-load on rock bolt using piezoceramic-transducer enabled time reversal method, *Sensors* 17 (11) (2017) 2467.

- [62] Comité Européen de Normalisation, Eurocode 2: design of concrete structures – Part 1.1: General rules and rules for buildings, CEN EN 1992-1-1:2004, 2004.
- [63] Comité Euro-International du Béton, Model Code 1990, Design code, CEB-FIP, 1990.
- [64] M.E.M. Mahroug, Behaviour of continuous concrete slabs reinforced with frp bars: experimental and computational investigations on the use of basalt and carbon fibre reinforced polymer bars in continuous concrete slabs, *Compos. B Eng.* 66 (4) (2014) 348–357.
- [65] ACI Committee, ACI 440.1R-03 Guide for the design and construction of concrete reinforced with FRP bars, Farmington Hills: American Concrete Institute, 2003.
- [66] ACI Committee, ACI 440.1R-06 Guide for the design and construction of concrete reinforced with FRP bars, Farmington Hills: American Concrete Institute, 2006.
- [67] B. Benmokrane, O. Chaallal, R. Masmoudi, Flexural response of concrete beams reinforced with FRP reinforcing bars, *ACI Struct. J.* 93 (1) (1996) 46–55.
- [68] ACI Committee, ACI 440.1R-15 Guide for the design and construction of concrete reinforced with FRP bars, Farmington Hills: American Concrete Institute, 2015.
- [69] I.S.I.S. Canada, Reinforcing Concrete Structures with Fibre Reinforced Polymers, Manitoba, ISIS Canada Corporation, Canada, 2001.